SIMULATION OF SUBSURFACE FLOWS ASSOCIATED WITH RAINFALL-INDUCED SHALLOW SLOPE FAILURES

Ching-Chuan Huang [1] and Chien-Li Lo [2]

ABSTRACT

Modeling transient subsurface flow along the soil-bedrock interface and the subsequent mounding of porewater pressure head in the slope toe zone is key to a successful prediction of rainfall-induced shallow slope failure and debris flow initiation. To this end, finite element analyses are performed on some model slopes subjected to artificial rainfall using calibrated soil-water characteristic curves (SWCCs) and soil permeability functions (SPFs). Analytical results highlighted the importance of lateral subsurface flow in modeling rainfall-induced shallow slope failure, which cannot be adequately simulated using one-dimensional seepage models. Analytical results also revealed that the formation of a saturated zone and an outward subsurface flow over the entire length of the soil-bedrock interface signals rapid slope mass wasting. Results of a comparative study showed that an accurate modeling of time-dependent subsurface water table development requires modifications to the analytical boundary conditions induced by the wash-away of the slope toe. An accurate physical model of shallow slope failures requires further works to address this issue.

Key words: Shallow slope failure, rainfall, soil-water characteristic curve, soil permeability function, finite element analysis.

1. INTRODUCTION

Although analytical modeling for rainfall-induced slope failures has been attempted over the past two decades, a satisfactory description of shallow slope failure initiation in the source area has yet to be obtained. Previous studies of rainfall-induced shallow slope failures have generally revealed that:

1. Rainfall-induced shallow slope failures provide a major source of debris flows (Bouwer 1966; Baetens *et al.* 2009). Shallow source slope failures are caused by the penetration of the wetting front from the slope surface (Okimura and Ichikawa 1985; Dai *et al.* 1999; Zhang *et al.* 2000; Kim *et al.* 2004; Cho 2009), in conjunction with decreases of matric suction and the loss of apparent cohesion (Yoshida *et al.* 1991; Rahardjo *et al.* 1995; Springman *et al.* 2003; Blatz *et al.* 2004; Lade 2010). Therefore, modeling of wetting front propagation plays a key role in quantifying the temporal characteristics of shallow slope failures.
2. Perched groundwater tables over a geological discontinuity with lower permeability play an important role in activating shallow slope failures and debris avalanches (Iseda and Tanabashi 1986; Buchanan *et al.* 1990; Dai *et al.* 1999; Zhang *et al.* 2000; Gerscovich *et al.* 2006).
3. Soil-water characteristic curves (SWCC) and soil permeability functions pertinent to specific soils, along with numerical analysis tools, can be used to capture the timing of wetting front propagation and the resulting slope failures (Cai and Ugai 2004; Kim *et al.* 2004; Gerscovich *et al.* 2006; Cho 2009; Tu *et al.* 2009; Montrasio *et al.* 2009; Rahimi *et al.* 2010).

However, there are deficiencies associated with the methodologies and findings of the above-mentioned studies, leading to limited success substantiating practical applications:

4. The majority of the analytical model for wetting front propagation has been based on a one-dimensional (1-D) assumption (Tan *et al.* 2004), *i.e.*, a subsurface flow in (or against) the direction of gravitation. Field monitoring and experimental results indicated that lateral (preferential) flows prevail in the hillslope (Anderson *et al.* 2009; Huang *et al.* 2009; Huang and Yuin 2010). Lateral flows in layered slope strata were observed in numerous studies (Weyman 1973; Pilgrim *et al.* 1978; Weiler and Naef 2003), but have rarely been considered in slope-stability-related analytical models.
5. The majority of the analytical model of slope stability was based on the assumption of infinite slope (Okimura and Ichikawa 1985; Pradel and Raad 1993; Rahardjo *et al.* 1995; Borga *et al.* 1998; Crosta 1998; Enoki 1999; Collins and Zndarcic 2004; Kim *et al.* 2004; Meisina and Scarabelli 2007; Lu and Godt 2008; Cho 2009; Lee *et al.* 2009; Godt *et al.* 2009; Montrasio *et al.* 2009) for which a phreatic line is parallel to the slope surface. However, numerous field studies have shown that shallow slopes consisting of colluvial deposits are often chair-shaped, *i.e.*, a relatively gentle slope around the toe that forms a self-stabilizing mechanism (Lumb 1975; Johnson and Sitar 1990; Jiao *et al.* 2005; Gercovich *et al.* 2006; Lacerda 2007; Cascini *et al.* 2008). Recent experimental evidence has shown the critical role of slope toe stability in seepage-caused slope failures and debris discharge (Orense *et al.* 2004; Chu-Agor *et al.* 2008; Huang *et al.* 2008; 2009; Huang and Yuin 2010). Analytical studies (Iverson and Major 1986; Reid and Iverson 1992) also indicated that seepage in slopes might introduce upward seepage force around the slope toe, causing static liquefaction, rather than shear failure, in that zone.

Manuscript received June 17, 2013; revised October 16, 2013; accepted October 18, 2013.

[1] Professor (corresponding author), Department of Civil Engineering, National Cheng Kung University, Tainan, Taiwan (e-mail: samhcc@mail.ncku.edu.tw).

[2] Assistant Professor, Department of Architecture and Environmental Design, Shu-Te University, Kaohsiung, Taiwan.

A successful modeling of rainfall-induced slope failures should be able to address issues stated in (4) and (5) above. The present study creates a preliminary phase for a new finite shallow slope failure model with coupled hydraulic and mechanical analyses. The focus of this study is on the accuracy of subsurface hydrologic modeling and possible influence of the boundary condition change induced by progressive failures of the slope.

2. MECHANISMS OF RAINFALL-INDUCED SHALLOW SLOPE FAILURES

The tested slopes consisted of a soil classified as SM (silty sand) according to the Unified Soil Classification System (USCS; ASTM D 2487). The soil is identical to that used in the large-scale and small-scale model slope tests reported by Huang *et al*. (2008, 2009) and Huang and Yuin (2010). Figure 1 schematically shows a cross section of the model slope, which was brought to failure by using a spatially and temporarily uniform artificial rainfall facility. "Shallow slope failure" is used in the following to depict a failure pattern that develops along the soil-bedrock interface located at a certain depth of a finite slope. This definition is different from the "shallow failure" conventionally used for infinite slopes. A 2.29 m long, 0.84 m high, and 0.645 m wide wooden soil bin made of 20 mm-thick plywood plates with waterproof coating was established (Fig. 1). The bin had a debris discharge collection funnel immediately below the slope toe. The debris collection bucket beneath the funnel was replaced during the artificial rainfall test at variable rates of 1 ~ 3 min. per bucket, depending on the discharging rate during the test. Sandy slopes were constructed by lightly compacting a specific weight of silty sand with a water content (ω) of 10% down into 20 mm-thick horizontal layers using a 0.45 N rubber hammer. This process was repeated until a 0.84-m-high sandy slope was completed. Locations of the moisture sensors along the central line of the slope are denoted as M1 ~ M11 in Fig. 1. The moisture sensors (Decagon, ECH2O) were 100 mm long, 10 mm wide, and 1 mm thick. The piezometers (KYOWA BPR-A-50KPS), denoted by P1, P2, and P3 in Fig. 1, had a capacity of 50 kPa and a high resolution of 0.04 kPa (or a resolution of 4 mm water head). Details of the construction procedure, soil moisture and piezometric measurements have been thoroughly described by Huang and Yuin (2010).

It should be noted that experimental works similar to those described in Fig. 1 with a similar focus on the internal soil moisture and porewater pressure response to rainfall were reported by Montrasio and Valentino (2007) and Sharma and Nakagawa (2010). It is widely known that the influence of side-wall friction to the behavior of model slopes and walls via the so-called "arching effect" is significant for the model with a small width-to-height ratio. In the case of a rainfall-induced shallow slope failures and debris flow-related model tests, slope failures and debris discharge are usually associated with "flow-like" slope material for which the arching effect is unlikely to prevail. This speculation is supported by past model tests reported by Okura *et al*. (2002) and Lourenco *et al*. (2006) who used model slopes with width-to-height ratios between 1.0 and 0.75, respectively. The model slope studied here has a higher width-to-height ratio of 1.34 comparing with the above-mentioned tests. Therefore, the effect of side wall friction to the observed slope behavior is assumed negligibly small in the present study.

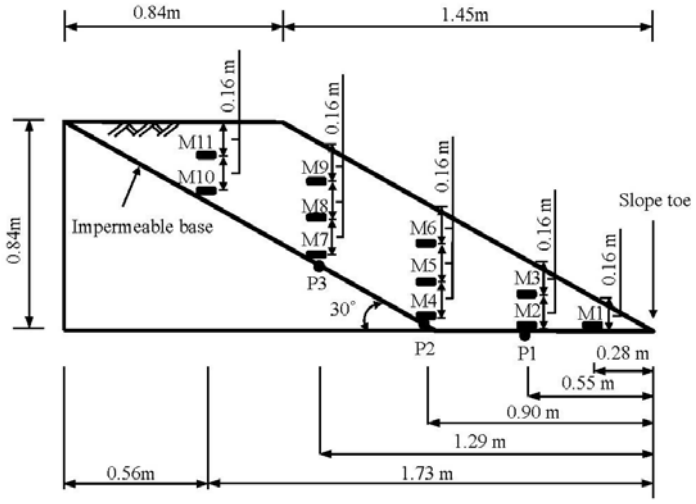

Fig. 1 Geometries of the model slope and locations of soil moisture and water pressure sensors in the tests reported by Huang and Yuin (2010)

Figures 2(a) ~ 2(d) show four typical moments of the model slope around the transition from a negligibly small debris discharge state into a measurable debris discharge state, for a slope subjected to a spatially and temporarily uniform rainfall intensity of I = 47 mm/hr. At time t = 74 min. after the beginning of rainfall, the slope was subjected to a minor toe failure, as shown in Fig. 2(a). Figs. 2(b), 2(c), and 2(d) show the retrogressive failures at t = 93 min., 103 min. and 133 min. respectively. The distinctive progress of a slumped area can be seen between t = 103 min. and t = 133 min. It can be seen in Figs. 2(c) and 2(d) that the slumped debris deposited around the slope toe had a gentle repose angle of about 15° ~ 18°. Figure 3 shows the cumulative debris discharge (Q_s) vs. time (t) curves for model slopes subjected to various spatially and temporally constant artificial rainfall with intensities of I = 23, 47, and 65 mm/hr. It can be seen that these curves are characterized by various transition points from a minor solid discharge state into a rapid discharge state. The slopes of these curve are also influenced by the value of the rainfall intensity. It should be noted that a transition period between a low discharge rate and a high discharge rate occurs between t = 103 and 133 min., as can be seen in Fig. 3 for the case of I = 47 mm/hr. Figure 4 shows various extents of slope failures (in terms of P_v defined as the percentage of discharged solid volume to the total volume of solids in an intact slope) subjected to I = 47 mm/hr. The porewater pressure heads along the impermeable base at specific times (t = 103, 133, 154, and 200 min.) are also shown. A significant mounding of the porewater pressure head between t = 103 and 133 min. can be seen, and after t = 133 min. no significant change of porewater pressure can be seen. In the debris discharge curve for I = 47 mm/hr in Fig. 3, the onset of rapid debris discharge is associated with a rapid porewater pressure head change in the slope toe zone. Figure 5 indicates the propagation of the wetting front from the slope surface to the base of the slope based on the soil moisture measured at S = 0.9 m

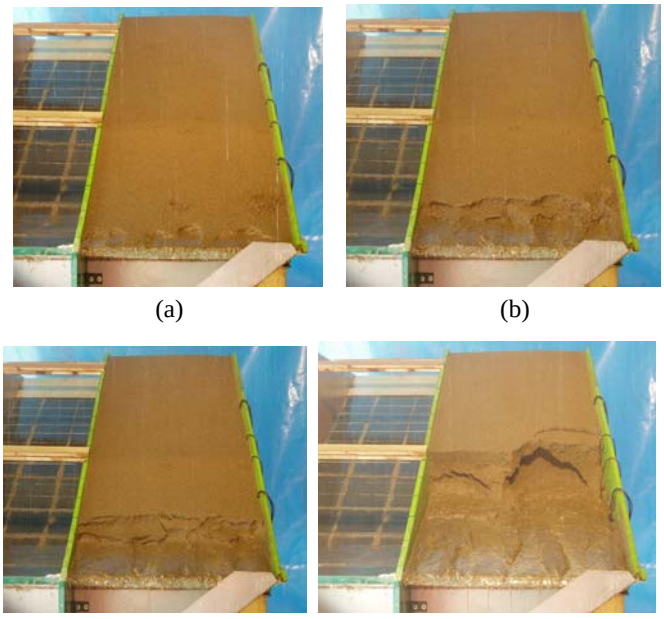

(a) (b) (c) (d)

Fig. 2 Various extents of slope failures in the artificial rainfall test (I = 47 mm/hr) reported by Huang and Yuin (2010), (a) A minor slope toe failure at t = 74 min; (b) A measurable slope toe failure at t = 93 min.; (c) An extensive slope toe failure at t = 103 min.; (d) A major slope failure at t = 133 min

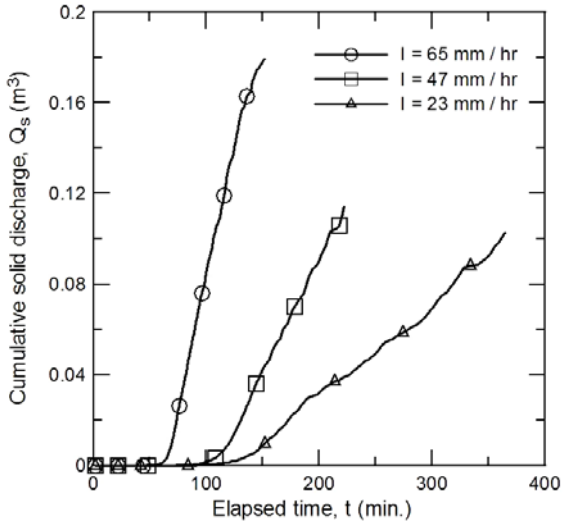

Fig. 3 Percentage of cumulative solid discharge vs. elapsed time between different rainfall intensity

(S: Horizontal distance from the slope toe). The soil moisture increases in the sequence M6 (at 0.16 m-deep) → M5 (at 0.32 m-deep) → M4 (at the impermeable base). Among them, the water contents of M6 increases from the initial state to saturation (ω = 0.27 ~ 0.30) within a very short period of time (between t = 75 and 80 min.), indicating that a saturated zone was formed locally after the arrival of the wetting front at the impermeable base. Note that the transition time of debris discharge (namely,

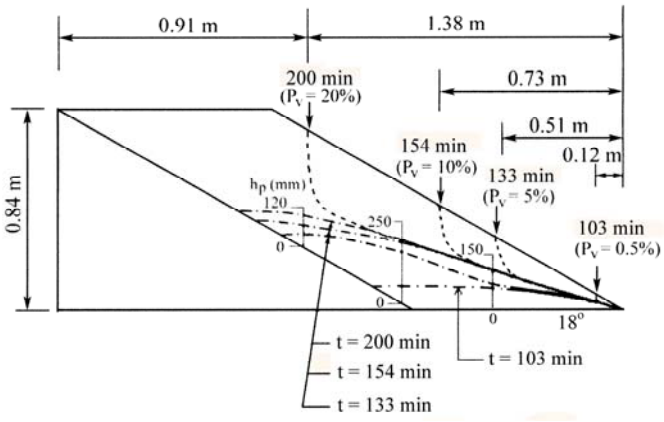

Fig. 4 Patterns of retrogressive failure and porewater pressure developments observed in the test of I = 47 mm/hr (after Huang and Yuin 2010)

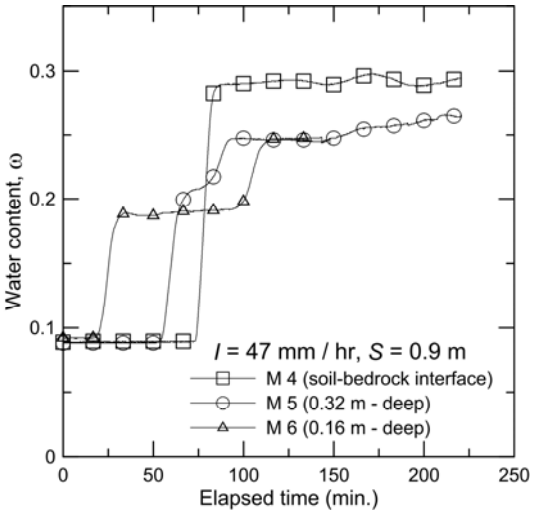

Fig. 5 Measured water content response at S = 0.9 m for the case of I = 47 mm/hr

t = 103 min. as shown in Fig. 3) is different from the transition time (t = 75 ~ 80 min.) of water content for M4, as shown in Fig. 5. This suggests that the time of wetting front arrival at a certain point of soil-bedrock interface precedes the formation of soil-bedrock interface flow which triggers the debris discharge. Figures 6(a) and 6(b) substantiate this view point in the sense that a saturated interface flow over the entire soil-bedrock interface occurs immediately after all points of measurement become saturated, which signals the launch of a saturated interface flow along the entire soil-bedrock interface and the debris discharge.

Figures 6(a) and 6(b) compare porewater pressures and soil water contents measured along the impermeable base at S = 0.55, 0.9, and 1.29 m. It is noted that the first transition point of soil moisture response curves always occurs before that for the porewater pressure response curve, suggesting a time-lag for porewater pressure response. The time-lag of porewater pressure response may be partially due to the limitation of the sensible range of piezometers. The measurement of piezometric head is

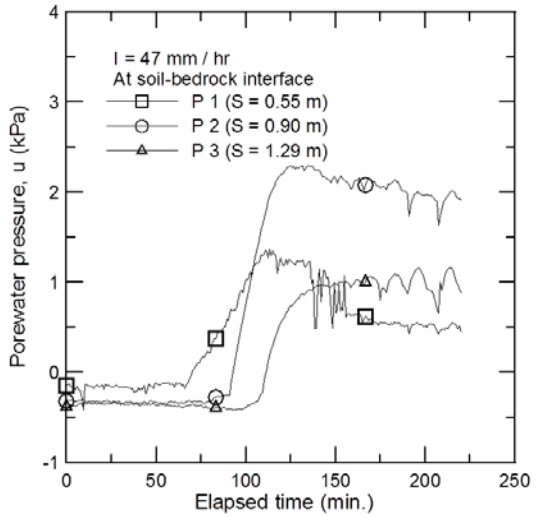

Fig. 6(a) Measured porewater pressure response for the test of I = 47 mm/ hr

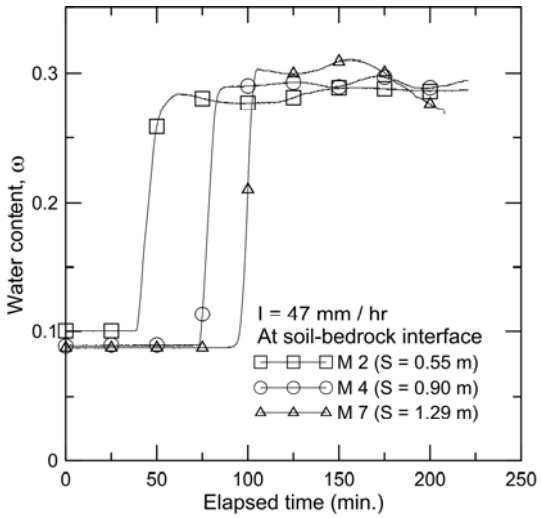

Fig. 6(b) Measured water content response at S = 0.55, 0.9, and 1.29 m (M2, M4, and M7) for the case of I = 47 mm/hr

more reliable in the case of positive porewater pressures. Transient and non-uniform distribution of suction around the ceramic cup of piezometers may account for the lagged detection. On the other hand, the moisture sensor is based on the dielectric constant of the medium, valid in sensing the moisture content change around the sensor up to the point of saturation. Therefore, these two types of sensors have different valid ranges (*i.e.*, the moisture sensor is valid for the pre-saturation state; the piezometer is valid for the post-saturation state), and are supplementary to each other. Based on the above observations, Fig. 7 schematically summarizes the mechanism of rainfall-induced shallow slope failures proposed by Huang and Yuin (2010), which was based on a series of artificial rainfall tests on various scales of model slopes consisting of sand with different void ratios as shown in Table 1 (Huang *et al*. 2008, 2009). The process of rainfall-induced shallow slope failure can be expressed in this sequence: ① vertical wetting front propagation through an unsaturated medium; ② wetting front arrives at impermeable bedrock; ③ lateral saturated flow occurs along the soil-bedrock interface; ④ lateral flow accumulates and initiate slope toe failures; ⑤ water table reaches a critical height associated with a rapid debris discharge. It was found that the moments of ③ ~ ④ were consistent with the moment of transition from a low debris discharge state to a high discharge state. The failure mechanism depicted in Fig. 7 is similar to that proposed by Take *et al*. (2004) for describing a slide-to-flow triggering mechanism of end-tipping loose fill slopes.

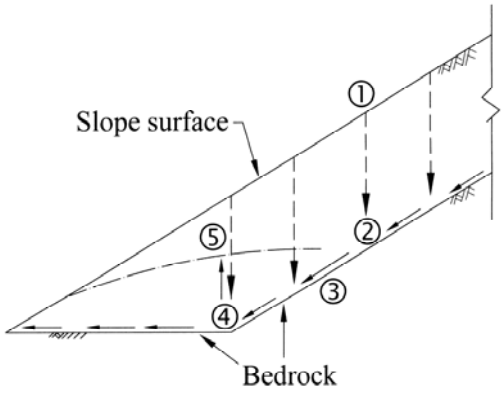

Fig. 7 Schematic model of subsurface flow propagation and phreatic water table mounding for a shallow slope subjected to rainfall infiltration proposed by Huang and Yuin (2010)

Table 1 The SWCC parameters for various conditions in the calibration box test

Void ratio, e	Relative density, D_r	Dry unit weight, γ_d (kN/m^3)	a	n	m
0.700	55%	15.2	4.4517	1.6238	1.6029
0.750	42%	14.7	4.9701	1.6543	1.8334
0.809	26%	14.2	5.0444	1.8133	1.9675
0.850	16%	13.9	5.1946	1.8565	2.1379

Note that the proposed model consisting of simplified initial and boundary conditions may not immediately applicable to natural slopes with complicate internal and / or external conditions, such as a perched water table which may generate a lateral seepage flow before the arrival of wetting front at soil-bedrock interface. Also note that this study focuses on the numerical simulation of wetting front propagation and a water table formation at the toe of the slope. Discussions on mechanical effects of slope failure and debris discharge, such as: The grain size and the dilatancy of the tested medium, is beyond the scope of this study.

3. MODELING SOIL-WATER CHARACTERISTICS CURVES

Figure 8 shows a cross section of the calibration box used for deriving the suction vs. water content relationships, namely the soil-water characteristic curve (SWCC). Test specimens were prepared using a sandy soil identical to that discussed for Fig. 1. Sand specimens with specific water content ω (= 0, 5%, 10%, 17.5%, and 25%) were statically compacted with 50 mm-thick lifts to achieve targeted dry unit weights of γ_d = 13.9, 14.2, 14.7,

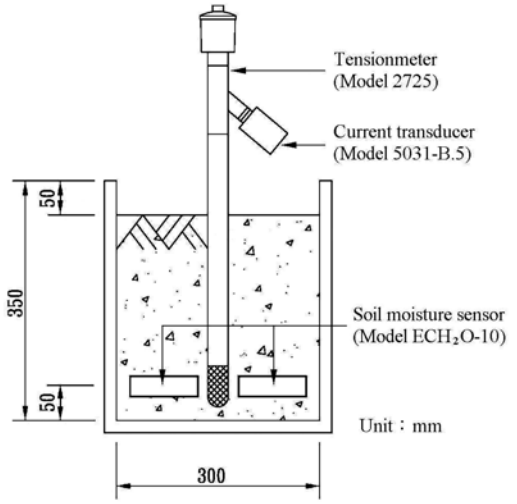

Fig. 8 One-dimensional seepage box used for deriving soil-water characteristic curves

and 15.2 kN/m^3 (or void ratios e = 0.850, 0.809, 0.750, and 0.700, respectively). A tensiometer (Model 2725 and 5031- B.5, Soilmoisture Equipment Corp.) was placed at the center of the box and two soil moisture sensors (Model ECH_2O-10, Decagon Devices, Inc.) were placed adjacent to the ceramic cup to measure the volumetric contents of the surrounding soils. These soil moisture sensors were calibrated prior to the test to ensure accurate water content measurements (Huang *et al*. 2008, 2009). To obtain the matric suction (ψ) vs. volumetric water content θ (= $\omega \cdot \gamma_d / \gamma_w$; γ_d: dry unit weight of sand, γ_w: unit weight of water) relationships for various void ratios of sand (as summarized in Table 1), a specific amount of water (2000 c.c.) was uniformly spread across the top surface of the soil specimen. The box was then covered with a plastic sheet for a certain period of time (for about 90 min.) until a new equilibrium state of soil moisture for the entire soil box was reached. The matric suction and soil moisture outputs were recorded at equilibrium states.

The use of 2000 c.c. of water for each step of water spreading was based on the result of trial-and-error tests. It was found that this amount of water generate detectable changes of volumetric water content of about 5% for each step of water spreading. Results of trial tests also showed that a smaller amount of water generated undetectable water content increase in the soil mass; a larger amount of water generated insufficient data points for the soil-water characteristic curve. A reversed operation for reducing the water content of the specimen using two 300-Watt heaters close to the top surface was performed to derive the ψ vs. θ relationships for the drying process. A small amount of hysteresis in ψ for about 2 kPa was found between the drying and wetting curves, which is consistent with the results reported by Fredlund and Rahardjo (1993). It should be noted that the present study focuses on the rainfall-induced failure mechanism observed in artificial rainfall tests, which is basically a wetting process. Therefore, only the wetting curves are used hereafter. Although a tensiometer measurement is not a standard test, it is a well-established method of in-field measurements. Various standard laboratory tests for deriving SWCC are with specific applicable ranges of matric suction (Nam *et al*. 2009). It is also difficult to obtain an entire range of matric suction for a SWCC using a single laboratory test method. Results of multiple types of laboratory tests with certain assumptions are usually required to determine a full-range SWCC. To alleviate this drawback, modern scientists and engineers can take the advantage of the well-established knowledge and database (*e.g.*, Arya and Paris 1981; Fredlund and Xing 1994; Aubertin *et al*. 2003), not just rely on standard tests in determining SWCCs. Most importantly, the SWCC based on the tensiometer measurement and the theoretical model of Fredlund and Xing (1994) used here has been carefully calibrated with a special focus on the wetting front propagation, reported in-detail by Huang *et al*. (2011). The experimental data can be curve-fitted using the equation for SWCC proposed by Fredlund and Xing (1994) as follow:

$$\theta = C(\psi) \cdot \frac{\theta_s}{\left\{ \ln\left[e + \left(\frac{\psi}{a} \right)^n \right] \right\}^m} \tag{1}$$

and

$$C(\psi) = 1 - \frac{\ln\left(1 + \frac{\psi}{\psi_r} \right)}{\ln\left(1 + \frac{10^6}{\psi_r} \right)} \tag{2}$$

where, ψ_r is the suction corresponding to the residual water content θ_r; ψ_r = 1500 kPa is used in the analysis, as suggested by Fredlund and Xing (1994); a, n, and m are curve-fitting parameters.

Figure 9 shows the experimental SWCCs for the same sand for two typical void ratios (namely, e = 0.7 and 0.85), expressed using the equation proposed by Fredlund and Xing (1994) with curve fitting parameters a, n, and m, as summarized in Table 1. Detailed descriptions on the equation of SWCC for the tested sand were provided by Huang *et al*. (2011).

4. MODELING SOIL PERMEABILITY FUNCTIONS

Based on the concept of relative permeability proposed by Burdine (1953) and the soil permeability models proposed by Childs and Collis-George (1950), Marshall (1958), and Kunze *et al*. (1968), Fredlund *et al*. (1994), proposed a soil permeability function (SPF), $k_u(\psi)$, based on the integration of the SWCC. Figure 10 shows a comparison of three SPFs for the wetting path of tested sand at e = 0.7. These curves were derived based on the fitted SWCC (as shown in Fig. 9), incorporated with the theories of SPF proposed by van Genuchten (1980), Green and Corey (1971), and Fredlund *et al*. (1994). It is noted that within the range of ψ = 1 ~ 100 kPa, the values of k_u provided by Fredlund *et al*. (1994) were the largest among three SPFs examined. Note that the range of matric suction between 1 and 100 kPa constitutes a steep segment of the SWCC as shown in Fig. 9. This means that soil permeability corresponding to this range of suction significantly influence the simulated seepage behavior of the tested medium. Detailed equations for various SPFs mentioned above have been provided by Huang *et al*. (2011).

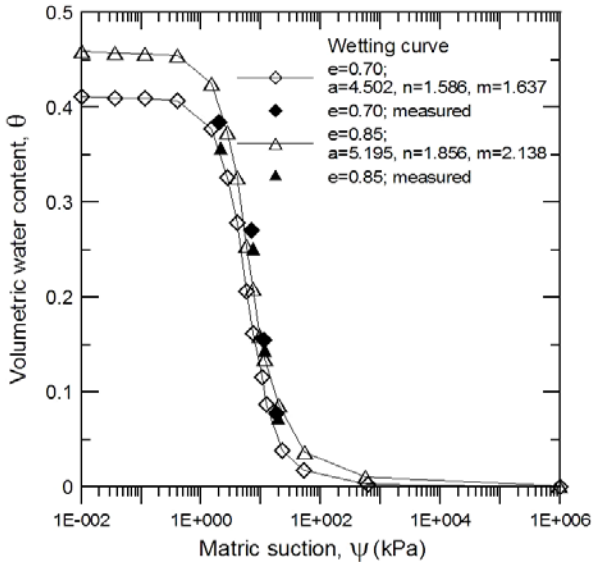

Fig. 9 Soil-water characteristic curves for various void ratios of sands used in the present study based on the model of Fredlund and Xing (1994)

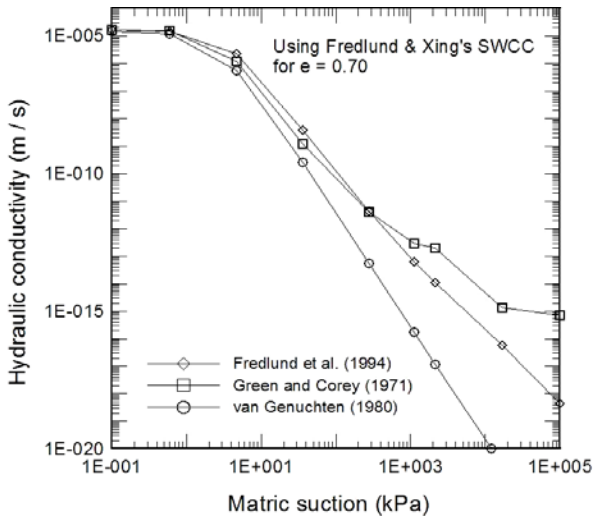

Fig. 10 Hydraulic conductivity functions for e = 0.70 based on the models proposed by Green and Corey (1971), van-Genutchen (1980) and Fredlund *et al.* (1994)

5. TRASIENT SEEPAGE ANALYSES

A computer program of finite element method (FEM), SEEP/W (Krahn 2004), was used to analyze the wetting front propagation and porewater pressure development of the model slopes subjected to artificial rainfall reported by Huang and Yuin (2010). The FEM program SEEP/W has also been used in a transient seepage analyses for two rainstorm-induced landslides, which incorporated a limit-equilibrium-based slope stability method (Casagli *et al*. 2006). In Casagli's study, empirical SWCCs and SPFs were used, thus contrasting to the calibrated SWCCs and SPFs used in the present study.

The transient seepage equation for two-dimensional (2-D), anisotropic, heterogeneous, unsaturated mediums based on the theorem of continuity of water phase and the assumption of negligible air flow influence in the FEM program can be expressed as:

$$\frac{\partial}{\partial x}\left[k_x \frac{\partial H}{\partial x}\right]+\frac{\partial}{\partial y}\left[k_y \frac{\partial H}{\partial y}\right]+q=\frac{\partial \theta}{\partial t}=m_w \gamma_w \frac{\partial H}{\partial t} \qquad (3)$$

where

k_x, k_y : Permeability coefficients in x and y directions, respectively

H : Total water head (= $u/\gamma_w + y$; u: pore water pressure; y: elevation)

γ_w : Unit weight of water

q : Boundary flux (in m/s)

m_w : Slope of θ vs. ψ curve

γ_w : Unit weight of water

In the present study, an isotropic condition, namely, $k_x = k_y = k_u(\psi)$, was assumed. Although anisotropic conditions ($k_x \neq k_y$) have been used in some parametric studies (*e.g.*, Ng and Shi 1998), this assumption was not strongly supported by experimental and field evidences. In addition, Witt and Brauns (1983) investigated the permeability anisotropy due to flatness and orientation of particles. They showed theoretically and experimentally that a randomly packed flat particles with a ratio of 4 (diameter):1 (thickness) was associated with $k_x / k_y = 2.3$. In view of the sub-rounded particle shape for the soil used in the present study, the permeability anisotropy is believed to be very small. The saturated permeability coefficients (k_s) used here were obtained based on a standard test method ASTM D 2434, and are summarized in Table 2. For the transient seepage analysis performed here, four-noded quadrilateral elements were used. A preliminary analysis of the wetting front propagation in a seepage box (to be discussed in the following section) showed a negligible advantage in using quadrilateral elements with more nodes. It is well-known that the accuracy of numerical calculations in time domain is ensured by using a small time increment. However, a too-small time increment entails unnecessarily long hour of calculations. To this end, a comparative study on the effectiveness of time intervals was conducted by using three time intervals (Δt), namely, 0.1 s, 1.0 s, and 5.0 s in a preliminary seepage analysis. Analytical results show that a decrease of time interval from 1.0 s to 0.1 s caused negligible influence on the rate of wetting front propagation and time of wetting front arrival. Therefore, a time increment of 1.0 s was used in the following analysis.

6. SEEPAGE ANALYSES USING FINITE ELEMENT METHOD

Figure 11 shows a cross section of the seepage test box and the locations of the soil moisture sensors. The soil specimen preparation method was identical to that used for the calibration box test described earlier. In this case constant water heads (Δh) of 10 mm or 50 mm were applied to the top surfaces of the soil specimens. Figure 12(a) shows the measured and simulated soil water content responses at a depth of 0.2 m. Four soil moisture sensors were installed at each depth (0.2 m and 0.42 m), and they all provided similar experimental curves. The analytical curves of Green and Corey (1971) and Fredlund *et al*. (1994) provided better results than those of van Genuchten (1980). This is attributable to the fact that the SPF based on the SWCC of van Genuchten (1980) generally has lowest values of $k_u(\theta)$ among three SPF curves examined in Fig. 10.

Table 2 Saturated soil permeability (k_s) for the tested soil with various void ratios

e	k_s[(1)] (m/s)
0.700	2.00×10^{-5}
0.750	3.60×10^{-5}
0.809	6.50×10^{-5}
0.850	9.32×10^{-5}

(1) Based on standard test method (ASTM D 2434)

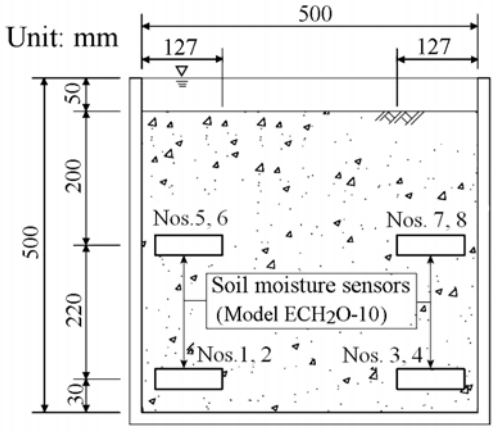

Fig. 11 One-dimensional seepage box with moisture sensors

Note that none of them successfully simulated post-peak water content reduction behavior. This can be attributed to the limitation of the analytical model in which the air-phase flow was not considered. To simultaneously simulate the water and air phases correctly, a rigorous approach such as that proposed by Fredlund and Rahardjo (1993) is necessary. Figure 12(b) describes θ vs. t relationships measured at the depth of 0.42 m for the test with e = 0.75 and Δh = 10 mm. It can be seen that the water content response at the depth of 0.42 m was well simulated using the SPF proposed by Fredlund *et al*. (1994). It can be seen in Fig. 12(b) that no post-peak reduction of θ was observed at the depth of 0.42 m, which is close to the base of the box. At this depth, the soil becomes 'flooded' or 'saturated' immediately after the arrival of wetting front. This is different from the middle depth of 0.2 m, where trapped air bubbles existed. Based on the result of comparative study shown in Figs. 12(a) and 12(b), SPFs of Fredlund *et al*. (1994) are used in the following analyses.

7. NUMERICAL ANALYSES ON WETTING FRONT PROPOGATION IN SHALLOW SLOPES

Figure 13 shows the geometry of the grids and boundary conditions used in the FEM analysis. The simulated model sandy slope is identical to those shown in Fig. 1. The input flux at the crest of the slope $q = 1.305 \times 10^{-5}$ m/s (= 47 mm/hr × 1 hr/3600 s × 10^{-3} m/mm) is an alternative expression of rainfall intensity, I. The input flux at the slope surface is obtained by projecting q (= 1.305×10^{-5} m/s) to the slanted slope surface (with a slope angle

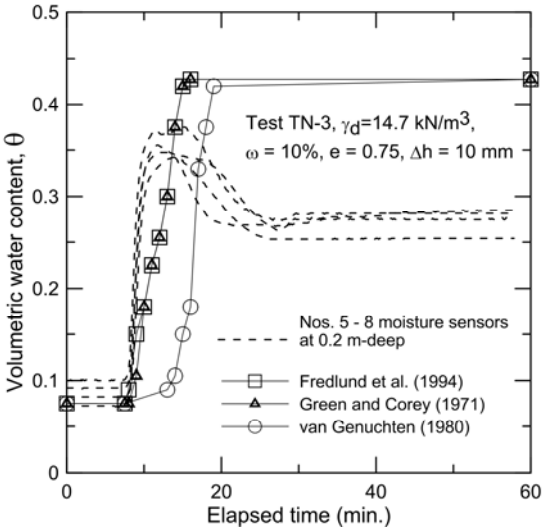

Fig. 12(a) Water content response at 0.2 m-depth in 1-D seepage tests

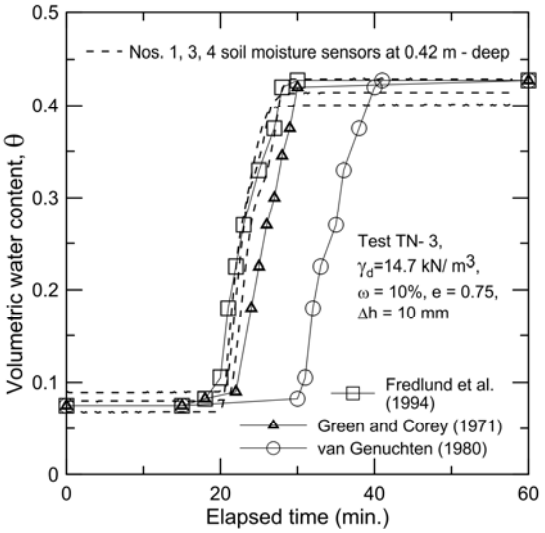

Fig. 12(b) Water content response at 0.42 m-deep in 1-D seepage tests

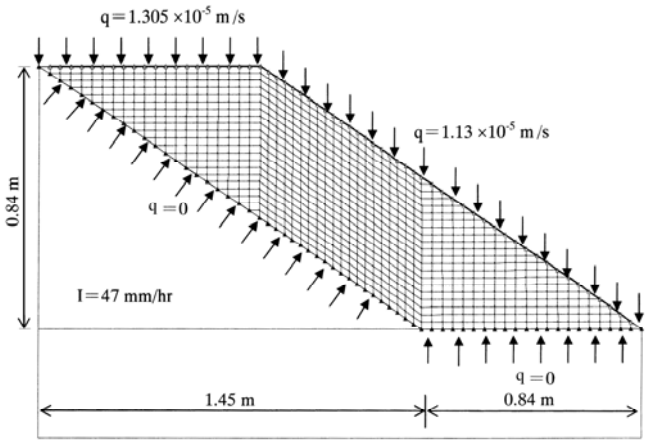

Fig. 13 Four-node quadrilateral finite grids and boundary conditions for the model slope subjected to a constant-intensity artificial rainfall of I = 47 mm/hr, reported by Huang and Yuin (2010)

of 30°), *i.e.*, the input flux at the slanted slope surface $q = 1.305 \times 10^{-5}$ m/s × cos 30°= 1.13×10^{-5} m/s. The size of the grids was determined based on a trial-and-error analysis of wetting front propagation and groundwater table development. A larger grid size was first used in the analysis and the results of the analyses in terms of the moisture content and porewater pressure head vs. time relationships were recorded. The grid size was gradually reduced in the next analysis and improved moisture and porewater head vs. time relationships were thus obtained and were compared with the previous ones. This process was repeated until no significant changes in the results could be obtained by reducing the grid size. Figures 14(a) ~ 14(c) show typical analytical results, expressed in contours of degree of saturation (S_r) at t = 74 min., 93 min., and 103 min., respectively. These times correspond to some significant moments when the slope was subjected to rainfall as shown in Figs. 2(a) ~ 2(c). There are some points that should be noted:

At t = 74 min. (Fig. 14(a)), vectors of seepage velocity in the slope toe zone were directed inside of the slope, and a minor zone of saturation was observed around the slope. This is consistent with the observed moisture and piezometric responses at the soil-bedrock interface, which showed no sign of wetting front arrival at t = 74 min. However, this is not the case for the seepage velocity vectors at t = 93 and 103 min., which show an outward lateral flow resulting from porewater pressure mounding in the slope toe zone. This suggests that the outward subsurface flow was non-existent until t = 93 min. which is close to the time of rapid debris discharge initiation at $t \fallingdotseq 103$ min. Lateral flows occur locally during this stage, *i.e.*, an overall lateral flow along the full length of the slope does not occur during this stage. This observation is supported by the analytical flow velocity field to be shown later.

At t = 74 min. positive piezometric heads were found only at the tip of the slope toe. At t = 93 and 103 min., the line of $S_r \geq 95\%$ (near-saturation state) developed nearly parallel to the slope base, *i.e.*, the lines of $S_r \geq 95\%$ formed a 'chair-shape' similar to that of the soil-bedrock interface. The formation of a nearly saturated zone over the entire interface signals the initiation of a lateral flow along the soil-bedrock interface, and is also consistent with the observation made in (1).

It can be seen in Fig. 14(c) that at t = 103 min., a significantly piezometric head higher than the measured one was obtained from the analysis. This contradiction is partially attributable to the unrealistic boundary used in the analysis. It can be seen in Fig. 2(c) that at t = 103 min., the toe of the slope experienced a substantial local washout. This was ignored in the analysis and is to be discussed further later.

Two-dimensional (2-D) analyses automatically account for the lateral subsurface flow which plays a vital role in addressing the failure mechanism of the slope toe. It is apparent that one-dimensional (1-D) seepage analyses is inadequate in addressing such an issue, because such analyses generate no information on the lateral subsurface flow.

8. EFFECTS OF BOUNDARY CONDITIONS ON THE PORE PRESSURE INCREASE

Figure 15(a) shows a comparison of calculated and measured porewater pressure heads at t = 133 min. for the case of

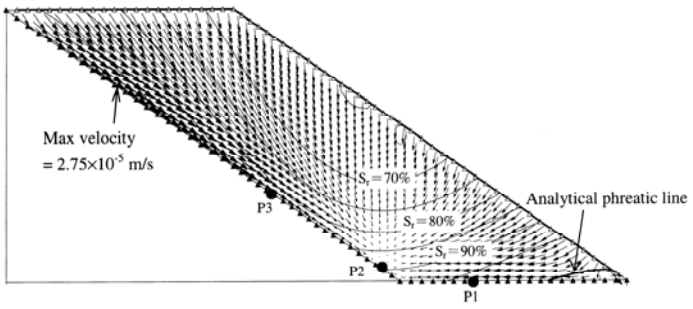

(a) at t = 74 min

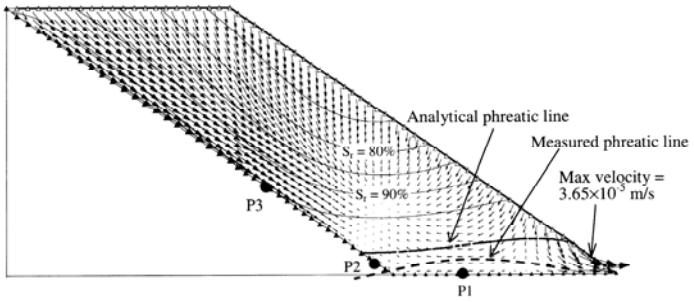

(b) at t = 93 min

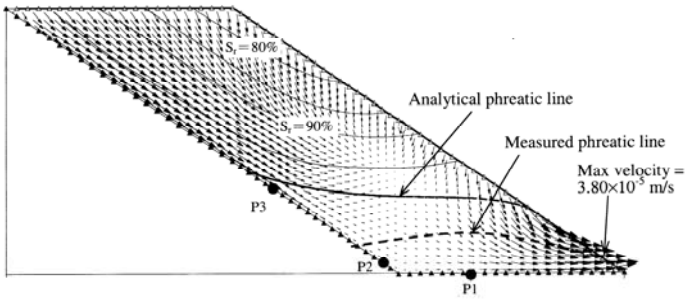

(c) at t = 103 min

Fig. 14 Vectors of seepage velocity obtained from the FEM analysis for the test of I = 47 mm/hr

I = 47 mm/hr. It is clear that the discrepancy between these two curves is great. In general, the difference between the calculated and the measured porewater pressure heads increases with the elapsed time. A parametric study on the SWCC and SPF is a good way of exploring possible factors accounted for the discrepancy between the observed and calculated results shown in Figs. 14(b) and 14(c). This approach was not employed in the present study, because the parameters of SWCC and SPF used here are results of a careful calibration as described in Figs. 8 ~ 12. The present study highlights one of the possible reasons, namely, the 'transient slope toe boundary change' which has never been explored. Figure 15(b) shows a typical example of the progressive removal of elements from the slope toe at t = 93 min. to approximate the observed washed-away slope boundary, as shown in Fig. 4. To achieve this, a procedure was adopted by preserving the analytical outcome (namely, θ and H in which are solutions for Eq. 3) for a specific time step. A modification to the slope toe boundary to comply with that observed in the test was subsequently made. The preserved data were then used as the initial condition for the modified slope geometry. The above process was executed at t = 93, 103, and 133 min, where the slope toe boundary change had been accurately measured, as

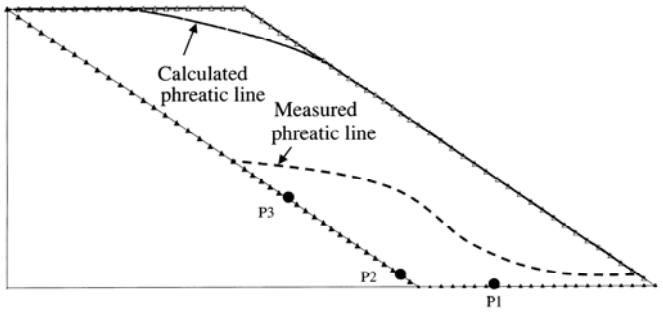

(a) Intact slope toe boundary

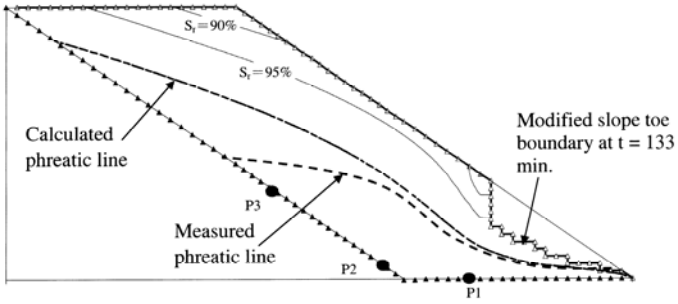

(b) Modified slope toe boundary

Fig. 15 Comparisons of measured at calculated porewater pressure heads for the test of I = 47 mm/hr at t = 133 min

shown in Fig. 4. It should be noted that removing the washed-away elements in the seepage analysis is a simplistic and preliminary way of investigating the effect of boundary condition changes around the slope toe. A more rigorous way of taking into account this effect is by performing a coupled analysis, which involves simultaneous seepage and stress analysis (*e.g.*, Fredlund and Rahardjo 1993; Carcia *et al*. 2011). This will be necessary in the future.

Figure 16(a) shows a comparison of measured and calculated values of porewater pressure (u) vs. t curves. Good agreement in terms of critical times where there is an abrupt increase in "u" can be seen. However, the calculated values of u tend to become overestimated after specific times. This overestimated value of "u" comes from ignoring the toe wash-out-induced boundary changes, as mentioned earlier. Figure 16(b) shows a comparison similar to that shown in Fig. 16(a), except the calculated porewater pressure heads are based on slope toe geometry modified by removal of some washed-away elements. It can be seen the agreement between the experimental and the simulated porewater pressure responses greatly improved, in the sense that final portions of the calculated u vs. t curves exhibit post-peak patterns that agree well with the observed ones.

9. CONCLUSIONS

Current slope stability models provide insufficient information about rainfall-induced subsurface hydrology regarding lateral flow along the soil-bedrock interface. To this end, the internal hydrological process for a shallow sandy slope subjected to artificial rainfall was investigated using finite element method (FEM), along with calibrated soil-water characteristic curves (SWCCs) and soil permeability functions (SPFs). The following conclusions were obtained:

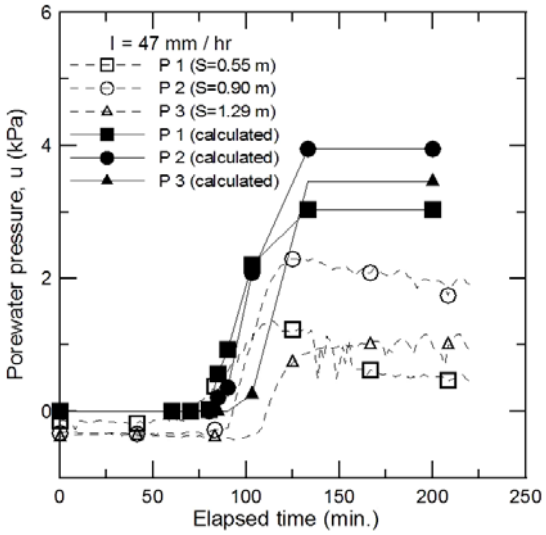

Fig. 16(a) Comparisons of measured and calculated porewater pressure responses for the test of I = 47 mm/hr

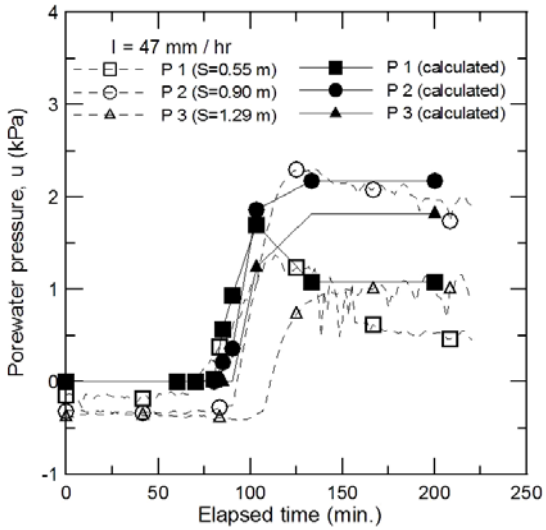

Fig. 16(b) Comparisons of measured and calculated porewater pressure responses for the modified slope subjected to I = 47 mm/hr

1. SWCCs for a silty sand were measured using tensiometers and soil moisture measurements. Results of finite element analyses suggest that the SWCCs and SPFs proposed by Fredlund and Xing (1994) and Fredlund *et al*. (1994), respectively, with calibrated parameters well-simulated the wetting front propogation observed in the calibration box and model slope tests.
2. Good agreements between the measured and analytical soil moisture response curves along the soil-bedrock interface were obtained. They all showed abrupt increases in soil moisture and porewater pressure at the time of wetting front arrival. This is associated with a saturated zone over the entire length of soil-bedrock interface. This facilitates a subsurface flow along the soil-bedrock interface and porewater pressure mounding at slope toe. The time of overall saturated zone formation was consistent with that of a lateral subsurface flow formation, and also the time of rapid debris discharge initiation.

3. Both analytical and measured results showed significant increases in piezometric heads around the toe of the slope at the initiation of rapid debris discharge. The difference between the analytical and measured porewater pressure heads became large as the extent of the slope failure increased because of less realistic analytical boundary conditions of the slope toe. Therefore, simulating the slope toe boundary change associated with the washing-away of slope mass plays a significant role in accurately modeling the internal moisture and piezometric responses of the slope. A coupled mechanical and seepage analysis incorporating a boundary change technique is necessary in the future to address this issue.

The conclusion derived here can be used to improve current practice which addresses the failure of the slope using a deterministic approach, ignoring the progressive failures of the slope toe and the retrogressive development of the slumped soil mass. To apply the discussed phenomenon to a real slope, it is necessary to identify numerous variable factors, such as the non-uniformity of soils, real-time groundwater table changes, real-time slope profile changes, *etc*. Obtaining such information for a real slope involves intensive undisturbed sampling, sophisticate monitoring, and high costs. In the future, verification of the proposed method using well monitored large-scale slope tests is suggested.

REFERENCES

Anderson, A. E., Weiler, M., Alila, Y., and Hudson, R. O. (2009). "Subsurface flow velocities in a hillslope with lateral preferential flow." *Water Resources*, **45**, W11407.

Arya, L. M. and Paris, J. F. (1981). "A physioempirical model to predict the soil moisture characteristics from particle-size distribution and bulk density data." *Soil Science Society American Journal*, **45**, 1023–1030.

ASTM D2434. *Standard Test Method for Permeability of Granular Soils (Constant Head)*. ASTM International, West Conshohocken, PA, USA.

ASTM D2487. *Standard Classification of Soils for Engineering Purposes (Unified Soil Classification System)*. ASTM International, West Conshohocken, PA, USA.

Aubertin, M., Mbonimpa, M., Bussiere, B., and Chapuis, R. P. (2003). "A model to predict the water retention curve from basic geotechnical properties." *Canadian Geotechnical Journal*, **40**, 1104–1122.

Baetens, J. M., Verbist, K., Cornelis, W. M., Gabriels, D., and Soto, G. (2009). "On the influence of coarse fragments on soil water retention." *Water Resources Research*, **45**, W07408, doi: 10,1029/2008WR007402.

Blatz, J. A., Ferreira, N. J., and Graham, J. (2004). "Effects of near-surface environmental conditions on instability of an unsaturated soil slope." *Canadian Geotechnical Journal*, **41**, 1111-1126.

Borga, M., Fontana, G. D., Ros, D. D., and Marchi, L. (1998). "Shallow landslide hazard assessment using a physically based model and digital elevation data." *Environmental Geology*, **35**, 81–88.

Bouwer, H. (1966). "Rapid field measurement of air entry value and hydraulic conductivity of soil as significant parameters in flow." *Water Resources Research*, **2**(4), 729–738.

Buchanan, P., Savigny, K. W., and Vries, J. DE. (1990). "A method for modeling water tables at debris avalanche headscarps." *Journal of Hydrology*, **113**, 61–88.

Burdine, N. T. (1953). "Relative permeability calculation size distribution data." *Transactions of the American Institute of Mining. Metallurgical, and Petroleum Engineers*, **198**, 71–78.

Cai, F. and Ugai, K. (2004). "Numerical analysis of rainfall effects on slope stability." *International Journal of Geomechanics*, **4**(2), 69–78.

Casagli, N., Dapporto, S., Ibsen, M. L., Tofani, V., and Vannocci, P. (2006). "Analysis of the landslide triggering mechanism during the storm of 20th-21st November 2000, in Northern Tuscany." *Landslides*, **3**, 13–21.

Cascini, L., Cuomo, S., and Guida, D. (2008). "Typical source areas of May 1998 flow-like movements in the Campania region, Southern Italy." *Engineering Geology*, **96**, 107–125.

Childs, E. C. and Collis-George, G. N. (1950). "The permeability of porous materials." *Proceedings, Royal Society of London*, Series A. **201**, 392–405.

Cho, S. E. (2009). "Infiltration analysis to evaluate the surficial stability of two-layered slopes considering rainfall characteristics." *Engineering Geology*, **105**, 32–43.

Chu-Agor, M. L., Fox, G. A., Cancienne, R. M., and Wilson, G. V. (2008). "Seepage caused tension failures and erosion undercutting of hillslopes." *Journal of Hydrology*, **359**, pp. 247–2590.

Collins, B. D. and Znidarcic, D. (2004). "Stability analyses of rainfall induced landslides." *Journal of Geotechnical and Geoenvironmental Engineering*, ASCE, **130**(4), 362–372.

Crosta, G. (1998). "Regionalization of rainfall thresholds: An aid of to landslide hazard evaluation." *Environmental Geology*, **35**, 131–145.

Dai, F., Lee, C. F., and Wang, S. (1999). "Analysis of rainstorm-induced slide-debris flows on natural terrain of Lantau Island, Hong Kong." *Engineering Geology*, **51**, 279–290.

Enoki, E. (1999). "Slope surface failure caused by precipitation. Tsuchi-To-Kiso." *Japanese Geotechnical Society*, **47**(5), pp. 17–20 (in Japanese).

Fredlund, D. G. and Rahardjo, H. (1993). *Soil Mechanics for Unsaturated Soils*, John-Willey & Sons, Inc.

Fredlund, D. G. and Xing, A. (1994). "Equations for the soil-water characteristic curve." *Canadian Geotechnical Journal*, **31**, 521–532.

Fredlund, D. G., Xing, A., and Huang, S. (1994). "Predicting the permeability function for unsaturated soils using the soil-water characteristic curve." *Canadian Geotechnical Journal*, **31**, 533–546.

Garcia, E., Oka, F., and Kimoto, S. (2011). "Numerical analysis of a one-dimensional infiltration problem in unsaturated soil by a seepage-deformation coupled method." *International Journal for Numerical and Analytical Methods in Geomechanics*, **35**, 544–568.

Gerscovich, D. M. S., Vargas, E. A., and de Campos, T. M. P. (2006). "On the evaluation of unsaturated flow in a natural slope in Rio de Janeiro, Brazil." *Engineering Geology*, **88**, 23–40.

Godt, J.W., Baum, R.L. and Lu, N. (2009). Landsliding in partially saturated materials. Geophysical Research Letters 36, L02403.

Green, R.E. and Corey, J.C. (1971). Calculation of Hydraulic Conductivity: A further evaluation of some predictive methods. Soil Science Society America Proceedings, Vol.35, pp. 3–8.

Huang, C.-C., Ju, Y.-J., Hwu, L.-K., and Lee, J.-L. (2009). "Internal soil moisture and piezometric responses to rainfall-induced shallow slope failures." *Journal of Hydrology*, **370**(1-4), 39–51.

Huang, C.-C., Lo, C.-L., Jang, J.-S., and Hwu, L.-K. (2008). "Internal soil moisture response to rainfall-induced slope failures and debris discharge." *Engineering Geology*, **101**(3-4), 134–145.

Huang, C.-C., Lo, C.-L., and Lan, S.-T. (2011). "An integrated approach for validating unsaturated soil parameters in seepage analyses." *Computers and Geotechnics*, **38**, 1089–1095.

Huang, C.-C. and Yuin, S.-C. (2010). "Experimental investigation of rainfall criteria for shallow slope failures.' *Geomorphology*, **120**, 326–338.

Iseda, T. and Tanabashi, Y. (1986). "Mechanism of slope failure during heavy rainfall in Nagasaki July 1982." *Natural Disaster Science*, **8**(1), 55–84.

Iverson, R. M. and Major, J. J. (1986). "Groundwater seepage vectors and the potential for hillslope failure and debris flow mobilization." *Water Resources Research*, **22**(11), 1543–1548.

Jiao, J. J., Wang, X.-S. and Nandy, S. (2005). "Confined groundwater zone and slope instability in weathered igneous rocks in Hong Kong." *Engineering Geology*, **80**, 71–92.

Johnson, K. A. and Sitar, N. (1990). "Hydrologic conditions leading to debris-flow initiation." *Canadian Geotechnical Journal*, **27**, 789–801.

Kim, J., Jeong, S., Park, S., and Sharma, J. (2004). "Influence of rainfall-induced wetting on the stability of slopes in weathered soils." *Engineering Geology*, **75**, 251–262.

Krahn, J. (2004). "Seepage modeling with SEEP/W: An engineering methodology." 1st Ed., Geo-Slope Internation, Ltd.

Kunze, R. J., Uehara, G., and Graham, K. (1968). "Factors important in the calculation of hydraulic conductivity." *Soil Science Society of America Proceedings*, **32**, 760–765.

Lacerda, W. A. (2007). "Landslide initiation in saprolite and colluviums in southern Brazil: Field and laboratory observations." *Geomorphology*, **87**, 104–119.

Lade, P. V. (2010). "The mechanics of surficial failure in soil slopes." *Engineering Geology*, **114**, 57–64.

Lee, L. M., Kassim, A., and Gofar, N. (2011). "Performances of two instrumented laboratory models for the study of rainfall infiltration into unsaturated soils." *Engineering Geology*, **117**, 78–89.

Lo, C.-L. (2009). "Study on the mechanism of rainfall-induced slope failure and debris discharge." *Ph. D. thesis*, Department of Civil Engineering, National Cheng Kung University, Taiwan.

Lourenco, S. D. N., Sassa, K., and Fukuoka, H. (2006). "Failure process and hydrologic response of a two layer physical model: Implications for rainfall-induced landslides." *Geomorphology*, **73**, 115–130.

Lu, N. and Godt, J. (2008). "Infinite slope stability under steady unsaturated seepage conditions." *Water Resources Research 44*, W11404.

Lumb, P. (1975). "Slope failure in Hong Kong." *Quarterly Journal of Engineering Geology*, **8**, 31–65.

Marshall, T. J. (1958). "A relation between permeability and size distribution of pores." *Journal of Soil Science*, **9**, 1–8.

Meisina, C. and Scarabelli, S. (2007). "A comparative analysis of terrain stability models for predicting shallow landslides in colluvial soils." *Geomorphology*, **87**, 207–223.

Montrasio, L. and Valentino, R. (2007). "Experimental analysis and modelling of shallow landslides." *Landslides*, **4**, 291–296.

Montrasio, L., Valentino, R., and Losi, G. L. (2009). "Rainfall-induced shallow landslides: A model for the triggering mechanism of some case studies in Northern Italy." *Landslides*, **6**, 241–251.

Nam, S., Gutierrez, M., Diplas, P., Petrie, J., and Wayllace, A. (2009). "Comparison of testing techniques and models for establishing the SWCC of riverbank soils." *Engineering Geology*, **110**, 1–10.

Ng, C. W. W. and Shi, Q. (1998). "A numerical investigation of the stability of unsaturated soil slopes subjected to transient seepage." *Computers and Geotechnics*, **22**(1), 1–28.

Okimura, T. and Ichikawa, R. (1985). "A prediction method for surface failures by movements of infiltrated water in surface soil layer." *Natural Disaster Science*, **7**(1), 41–51.

Okura, Y., Kitahara, H., Ochiai, H., Sammori, T., and Kawanami, A. (2002) "Landslide fluidization process by flume experiments." *Engineering Geology*, **66**, 65–78.

Orense, R. P., Shimoma, S., Maeda, K., and Towhata, I. (2004). "Instrumented Model slope failure due to water seepage." *Journal of Natural Disaster Science*, **26**(1), 15–26.

Pilgrim, D. H., Huff, D. D., and Steele, T. D. (1978). "A field evaluation of subsurface and surface runoff." *Journal of Hydrology*, **38**, 319–341.

Pradel, D. and Raad, G. (1993). "Effect of permeability on surficial stability of homogeneous slopes." *Journal of Geotechnical Engineering*, **119**, 315–332.

Rahardjo, H., Lim, T. T., Chang, M. F., and Fredlund, D. G. (1995). "Shear-strength characteristics of a residual soil." *Canadian Geotechnical Journal*, **32**, 60–77.

Rahimi, A., Rahardjo, H., and Leong, E. C. (2010). "Effect of hydraulic properties of soil on rainfall-induced slope failure." *Engineering Geology*, **114**, 135–143.

Reid, M. E. and Iverson, R. M. (1992). "Gravity-driven groundwater flow and slope failure potential 2. Effects of slope morphology, material properties, and hydraulic heterogeneity." *Water Resources Research*, **28**(3), 939–950.

Sharma, R. H. and Nakagawa, H. (2010). "Numerical model and flume experiments of single- and two-layered hillslope flow related to slope failure." *Landslides*, **7**, 425–432.

Springman S. M., Jommi, C., and Teysseire, P. (2003). "Instabilities on moraine slopes induced by loss of suction: A case history." *Geotechnique*, **53**(1), 3–10.

Take, W. A., Bolton, M. D., Wong, P. C. P., and Yeung, F. J. (2004). "Evaluation of landslide triggering mechanisms in model fill slopes." *Landslides*, **1**, 173–184.

Tan, T. S., Phoon, K. K., and Chong, P. C. (2004). "Numerical study of finite element method based solutions for propagation of wetting fronts in unsaturated soil." *Journal of Geotechnical and Geoenvironmental Engineering*, ASCE, **130**(3), 254–263.

Tu, X. B., Kwong, A. K. L., Dai, F. C., Tham, L. G., and Min, H. (2009). "Field monitoring of rainfall infiltration in a loess slope and analysis of failure mechanism of rainfall-induced landslides." *Engineering Geology*, **105**, 134–150.

Van Genuchten, M. Th. (1980). "A close-form equation for predicting the hydraulic conductivity of unsaturated soils." *Soil Science Society of America Journal*, **44**, 892–898.

Weiler, M. and Naef, F. (2003). "Simulating surface and subsurface initiation of macropore flow." *Journal of Hydrology*, **273**, 139–154.

Weyman, D. R. (1973). "Measurements of the downslope flow of water in a soil." *Journal of Hydrology*, **20**, 267–288.

Witt, K.-J. and Brauns, J. (1983). "Permeability-anisotropy due to particle shape." *Journal of Geotechnical Engineering*, **109**(9), 1181–1187.

Yoshida, Y., Kuwano, J., and Kuwano, P. (1991). "Rain-induced slope failures caused by reduction in soil strength." *Soils and Foundations*, **31**(4), 187–193.

Zhang, J., Jiao, J. J., and Yang, J. (2000). "In situ rainfall infiltration studies at a hillside in Hubei Province, China." *Engineering Geology*, **57**, 31–38.